Shock Tube and Theory Investigation of Cyclohexane and 1-Hexene Decomposition

J. H. Kiefer,*,† K. S. Gupte,† L. B. Harding,‡ and S. J. Klippenstein‡

Department of Chemical Engineering, University of Illinois at Chicago, Chicago, Illinois 60607, and Chemistry Division, Argonne National Laboratory, Argonne, Illinois 60439

Received: June 23, 2009; Revised Manuscript Received: September 4, 2009

The decomposition of cyclohexane (c-C_6H_{12}) was studied in a shock tube using the laser-schlieren technique over the temperature range 1300−2000 K and for 25−200 Torr in mixtures of 2%, 4%, 10%, and 20% cyclohexane in Kr. Vibrational relaxation of the cyclohexane was also examined in 10 experiments covering 1100−1600 K for pressures below 20 Torr, and relaxation was found to be too fast to allow resolution of incubation times. The dissociation of 1-hexene (1- C_6H_{12}), apparently the sole initial product of cyclohexane decomposition, was also studied over 1220−1700 K for 50 and 200 Torr using 2% and 3% 1-hexene in Kr. On heating, cyclohexane simply isomerizes to 1-hexene, and this then dissociates almost entirely by a more rapid C−C scission to allyl and *n*-propyl radicals. This two-step reaction results in an initial small density gradient from the slight endothermicity of the isomerization. The gradient then rises strongly as the product 1-hexene dissociates. For the lower temperatures, this behavior is fully resolved here. For the higher pressures, 1-hexene decomposition generates negative gradients (exothermic reaction) as the radicals formed begin to recombine. Cyclohexane also generates such gradients, but these are now much smaller because the radical pool is depleted by abstraction from the reactant. A complete mechanism for the 1-hexene decomposition and for that of cyclohexane involving 79 reactions and 30 species is used in the final modeling of the gradients. Rate constants and RRKM fit parameters for the initial reactions are provided for the entire range of conditions. The possibility of direct reaction to allyl and *n*-propyl radicals, without stabilization of the intermediate 1-hexene, is examined down to pressures as low as 25 Torr, without a clear resolution of the issue. High-pressure limit rate constants from RRKM extrapolation are k_∞(c-C_6H_{12} → 1-C_6H_{12}) = (8.76×10^{17}) exp((−91.94 kcal/mol)/*RT*) s^{-1} (*T* = 1300−2000 K) and k_∞(1-C_6H_{12} → $^{\bullet}C_3H_7$ + $^{\bullet}C_3H_5$) = (1.46×10^{16}) exp((−69.12 kcal/mol)/*RT*) s^{-1} (*T* = 1200−1700 K). This high-pressure rate for cyclohexane is entirely consistent with the notion that the isomerization involves initial C−C fission to a diradical. These extrapolated high-pressure rates are in good agreement with much of the literature.

Introduction

Cyclohexane (c-C_6H_{12}) is a common surrogate for cycloalkane fuels.[1−3] It is itself a common constituent in many conventional fuels and is especially an important constituent of the new generation of fuels derived from tar sands and shales.[2,4−6] In recognition of its importance to combustion chemistry, cyclohexane oxidation and pyrolysis have been widely studied. A fairly detailed review of prior studies is to be found in refs 2, 5, and 7. Despite the extensive previous effort, the actual product channels are still not fully agreed upon and convincing rate data are rather limited.

1-Hexene (1-C_6H_{12}) belongs to the class of olefins which are common intermediate species in alkane oxidation, as described in refs 8 and 9. However, the primary motivation behind the present study of 1-hexene dissociation, as will be confirmed later, lies in the fact that cyclohexane mainly isomerizes to 1-hexene at the experimental conditions of this study and this then dissociates faster than the cyclohexane. The 1-hexene dissociation is thus an essential part of the cyclohexane decomposition mechanism.

Pyrolytic studies of fuels are particularly important to the understanding of combustion because, at the higher combustion temperatures, the fuel will dissociate, initiating chain oxidation, and the modeling of this process naturally requires a reliable pyrolytic mechanism (for example, see refs 10 and 11). Thus, the objective of this study is an establishment of the dissociation channels in cyclohexane and a determination of rates for these for high combustion temperatures and moderate pressures. As part of this, a complete reaction mechanism for cyclohexane decomposition of 30 species and 79 reactions is proposed. After the mechanism is defined, a high-pressure-limit (k_∞) rate constant for the dominant initial isomerization step is finally obtained from the rate determinations using RRKM extrapolation.

The earliest modern observation of cyclohexane dissociation, at least for the high-temperature conditions appropriate to pyrolytic initiation, was that of Tsang.[12] His experiments used single-pulse shock tube heating together with a GC/FID (flame ionization detector) analysis of stable species and employed the dissociation of a chemical thermometer (cyclohexene) to determine temperature. Tsang determined that the only reaction channel around 1100 K was isomerization to 1-hexene:

$$\text{c-}C_6H_{12} \rightarrow \text{1-}C_6H_{12} \qquad (1)$$

On the basis of common trends seen in the dissociation of other cycloalkanes, Tsang also proposed a diradical pathway for this as in the following reactions:

* To whom correspondence should be addressed. E-mail: kiefer@uic.edu.
† University of Illinois at Chicago.
‡ Argonne National Laboratory.

10.1021/jp905891q CCC: $40.75 © 2009 American Chemical Society
Published on Web 10/20/2009

$$c\text{-}C_6H_{12} \rightarrow {}^{\bullet}CH_2(CH_2)_4CH_2{}^{\bullet}({}^{\bullet}C_6H_{12}{}^{\bullet}) \quad \text{(Ia)}$$

$${}^{\bullet}C_6H_{12}{}^{\bullet} \rightarrow 1\text{-}C_6H_{12} \quad \text{(Ib)}$$

[Reactions included in the recommended mechanism are identified with Arabic numerals and numbered according to the numbering in the full mechanism. Reactions identified with Roman numerals are considered here, but are not included in the final mechanism or in the reported calculations. The entire cyclohexane/1-hexene reaction mechanism is made available in the Supporting Information.] Tsang also complemented his work on cyclohexane dissociation by a separate study of 1-hexene pyrolysis.

More recently, Aribike et al.[13,14] studied cyclohexane dissociation in an annular flow reactor over 1000−1300 K with 1 atm of N_2 as the bath gas. They proposed the alternative reactions

$$c\text{-}C_6H_{12} \rightarrow 3C_2H_4 \quad \text{(II)}$$

$$c\text{-}C_6H_{12} \rightarrow 2C_3H_6 \quad \text{(III)}$$

$$c\text{-}C_6H_{12} \rightarrow C_4H_6 + C_2H_4 + H_2 \quad \text{(IV)}$$

whereas Tsang's proposed diradical pathway, reactions Ia and Ib, was supported by Brown and co-workers,[15] who studied the decomposition of cyclohexane at temperatures of 900−1200 K using the very low pressure pyrolysis (VLPP) technique. However, their estimated k_∞ for 1000 K is a factor of 4 higher than that reported by Tsang.[12]

Voisin et al.[16] studied cyclohexane oxidation in a jet-stirred reactor for 750−1100 K and 10 atm in cyclohexane/air mixtures at various equivalence ratios. In addition to channel II, they introduced a C−H fission channel:

$$c\text{-}C_6H_{12} \rightarrow {}^{\bullet}c\text{-}C_6H_{11} + H \quad \text{(V)}$$

El-Bakali et al.[17] also studied cyclohexane oxidation in a jet-stirred reactor over 750−1200 K using 1, 2, and 10 atm of cyclohexane/air mixtures at different equivalence ratios. A further diradical to molecular channel was suggested:

$$c\text{-}C_6H_{12} \rightarrow C_2H_4 + {}^{\bullet}C_4H_8{}^{\bullet} \quad \text{(IIa)}$$

$${}^{\bullet}C_4H_8{}^{\bullet} \rightarrow 2C_2H_4 \quad \text{(IIb)}$$

Granata et al.[18] introduced the further molecular channel

$$c\text{-}C_6H_{12} \rightarrow c\text{-}C_6H_{10} + H_2 \quad \text{(VI)}$$

McEnally et al.[19] studied cyclohexane pyrolysis in a coflowing, nonmixed CH_4/air flame doped with 2000 ppm cyclohexane covering 400−2000 K at 1 atm of pressure. On the basis of product analysis, rate expressions were suggested for channels 1, II, and V.

Most recently, Braun-Unkhoff et al.[20] investigated highly diluted cyclohexane pyrolysis in reflected shock waves using the H-atom ARAS technique to monitor the time-dependent H-atom concentration for $T = 1200-1900$ K and $P = 1.5-2$ bar of argon. Here reactions II and V were suggested as possible dissociation channels. There are also several other studies of the oxidation that have proposed similar pyrolytic mechanisms.[2,4,5,21,22]

In addition to all the experimental and simulation studies, a theoretical study has been presented by Sirjean et al.[23] using the CBS-QB3 method. They report that ring-opening in cyclohexane does indeed proceed through formation of a diradical intermediate, as in reaction Ia. Unimolecular rate constants for several following channels were calculated using transition-state theory, and overall rate constants were then determined by assuming a steady state for the diradical. In addition to reaction Ib, alternate channels for the diradical dissociation were

$${}^{\bullet}C_6H_{12}{}^{\bullet} \rightarrow C_2H_4 + {}^{\bullet}C_4H_8{}^{\bullet} \quad \text{(IIaa)}$$

$${}^{\bullet}C_6H_{12}{}^{\bullet} \rightarrow CH_2{=}CHCH_2CH_2CH_2CH_2{}^{\bullet} + H \quad \text{(VII)}$$

$${}^{\bullet}C_6H_{12}{}^{\bullet} \rightarrow C_3H_7\text{-}c\text{-}C_3H_5 \text{ (propylcyclopropane)} \quad \text{(VIII)}$$

$${}^{\bullet}C_6H_{12}{}^{\bullet} \rightarrow 2\ c\text{-}C_3H_6 \text{ (both cyclopropane)} \quad \text{(IX)}$$

None of these were found to be competitive with reaction Ib and thus were not included in further consideration.

Recognizing the numerous diradical conformers involved in reactions Ia and Ib, two schemes, labeled 7 and 8, were put forward. In Scheme 7, only the lowest energy diradical was considered, neglecting internal rotation barriers, whereas in Scheme 8, rotational hindrance in the diradical was explicitly considered. This work is considered more fully below.

As for 1-hexene, similar to other long-chain hydrocarbons, it mainly dissociates via C−C fission. Furthermore, in this and many other straight chain olefins, C−C bonds adjacent to allylic fragments, i.e., the C3−C4 bond in 1-hexene, are weakest and the preferred sites for fission. This notion is further supported by Tsang's study of products from 1-hexene dissociation.[12] Tsang's experiments cover 1000−1200 K and 2−5 atm using 0.01% 1-hexene with 1% toluene as the radical scavenger and argon as the bath gas. On the basis of the product analysis, he concluded that the dominant channel is

$$1\text{-}C_6H_{12} \rightarrow CH_3CH_2CH_2{}^{\bullet} + {}^{\bullet}CH_2CH{=}CH_2 \qquad \Delta H_f^{298K} = 75.15 \text{ kcal/mol} \quad (2)$$

while the contribution from the retro-ene (1,5 H-atom shift) channel

$$1\text{-}C_6H_{12} \rightarrow CH_3CH{=}CH_2 + CH_3CH{=}CH_2 \qquad \Delta H_f^{298K} = 19.74 \text{ kcal/mol} \quad (X)$$

to the overall rate was around 10−20%. This retro-ene channel is discussed again later in this paper.

1-Hexene dissociation was also studied by King[24] using the VLPP technique at 915−1153 K. Activation energies for reactions 2 and X (70.8 and 57.7 kcal/mol, respectively) were found by matching RRKM calculations to the VLPP data and were very similar to those obtained in Tsang's study[12] (70.7

and 57.4 kcal/mol, respectively). The *A* factors for reactions 2 and X were assigned from the results of Tsang,[12] and this, of course, resulted in rate constant expressions almost identical to those of Tsang.

In a recent study on the oxidation of 1-hexene, Yahyaoui and co-workers[8] measured autoignition delay times for 1-hexene/O_2/Ar mixtures between 1270 and 1700 K using a shock tube technique. Modeling was done using a reaction mechanism generated from the EXGAS[25,26] modeling code. At low temperatures (<1750 K), their model predicted reaction X as the dominant dissociation channel, whereas at higher temperatures a major contribution from reaction 2 was suggested. However, it seems unlikely that the retro-ene channel (reaction X) can be dominant over the entire temperature range of ref 8 because the bond fission activation entropy of reaction 2 is much higher than that of reaction X. This notion is further supported by Tsang's rate constants,[12] which predict that reaction X is a minor channel for temperatures above 1000 K. There are additional reasons for discounting reaction X, to be discussed below.

Our main purpose here is presentation and examination of new experimental results using the laser-schlieren (LS) technique in incident shock waves with the intent of establishing the correct reaction paths and rates for the decomposition of both 1-hexene and cyclohexane at the high temperatures involved in pyrolytic decomposition.

Experimental Section

The shock tube used in the LS experiments has a 4 ft long driver section of 4 in. i.d. connected to a 10 ft driver section of 2.5 in. i.d. whose detailed layout has been very fully described.[27] The ST/LS diagnostics have also been described previously.[28] The data acquisition system for the LS experiment has been upgraded, giving improved sensitivity and resolution, but again this has been fully described elsewhere.[29,30] In addition to the improved hardware, the control and analysis software has also been updated. This software determines chemically frozen, but vibrationally equilibrated, ideal-shock parameters and also calculates the Blythe and Blackman corrections[29−31] used in the conversion of relaxation in density to that of energy. As before,[27] velocities were set by interpolation of four intervals calculated from measured times centered about the LS beam. On the basis of extensive experience, the uncertainty in velocity is estimated as ±0.2%, corresponding to a temperature error of less than ±0.5%, here amounting to an error on the order of ±10 K. To produce the very weak shocks necessary for low-pressure dissociation and relaxation experiments, a slow flow of driver gas was achieved by introducing various converging/diverging nozzles of different throat diameters at the diaphragm. The experiments all used Mylar diaphragms of 0.002−0.005 in. thickness, burst spontaneously with helium.

For this study, 31 LS experiments on 2% and 3% 1-hexene/Kr mixtures at 1220−1700 K for 50 and 200 Torr, together with 131 experiments on 2%, 4%, 10%, and 20% cyclohexane/Kr mixtures at 1400−2000 K covering 25−200 Torr, were examined. The gas mixtures in these experiments were prepared using cyclohexane (purity 99.9+%) and 1-hexene (purity 99+%) from Sigma-Aldrich and krypton from Spectra Gases (excimer grade). Initial frozen reaction, relaxed vibration calculations assumed ideal-shock, ideal-gas behavior using the equilibrium thermodynamic data of Burcat and Ruscic.[32] Molar refractivities used in the calculation of the density gradient from measured angular deflection were 27.72 for cyclohexane,[33] 29.25 for 1-hexene,[33] and 6.367 for Kr.[34] The density gradient further along in the shock is calculated assuming that the molar refractivity of the mixture remains constant throughout the decomposition. This assumption is valid for high dilutions of test gases in bath gas Kr, but may need to be reassessed for experiments carried out with higher concentrations of test gases. To illustrate the effect of refractive variation, one high-temperature and high-fraction experiment (10% c-C_6H_{12} in Kr at $P_2 = 27$ Torr and $T_2 = 1905$ K) was selected. This experiment should serve as an upper bound on the deviation from the constant molar refractivity assumption. The experiment was simulated using the cyclohexane dissociation mechanism, and the refractivities of all the species in the reaction mixture were calculated using group additivity.[34] The refractivity of the reacted mixture was always found to be lower than that of the unreacted mixture. At a 5 μs laboratory time, effectively the full time normally considered in modeling, the deviation from the unreacted mixture refractivity was found to be only 9%. For a 2% c-C_6H_{12} in Kr mixture—the mixture used for most of the experiments—the deviation from initial refractivity did not exceed 4% even for the overly long reaction time of 10 μs.

Results and Discussion

1-Hexene. ***Possible Dissociation Channels.*** Fission can occur at any C−C single bond as in the following channels:

$$1\text{-}C_6H_{12} \rightarrow {}^{\bullet}CH_3 + {}^{\bullet}CH_2CH_2CH_2CH{=}CH_2 \qquad \Delta H_f^{298K} = 89.23 \text{ kcal/mol} \quad \text{(XI)}$$

$$1\text{-}C_6H_{12} \rightarrow CH_3CH_2^{\bullet} + {}^{\bullet}CH_2CH_2CH{=}CH_2 \qquad \Delta H_f^{298K} = 87.57 \text{ kcal/mol} \quad (3)$$

$$1\text{-}C_6H_{12} \rightarrow CH_3CH_2CH_2^{\bullet} + {}^{\bullet}CH_2CH{=}CH_2 \qquad \Delta H_f^{298K} = 75.15 \text{ kcal/mol} \quad (2)$$

$$1\text{-}C_6H_{12} \rightarrow CH_3CH_2CH_2CH_2^{\bullet} + {}^{\bullet}CH{=}CH_2 \qquad \Delta H_f^{298K} = 100.50 \text{ kcal/mol} \quad \text{(XII)}$$

C−H fission is also possible: of the numerous C−H fissions in 1-hexene the most likely is the one which forms the resonance-stabilized $^{\bullet}C_6H_{11}$ radical

$$1\text{-}C_6H_{12} \rightarrow CH_3CH_2CH_2{}^{\bullet}CHCH{=}CH_2 + H \qquad \Delta H_f^{298K} = 85.45 \text{ kcal/mol} \quad \text{(XIII)}$$

Bond fission channels usually have barriers near their heats of reaction. Here the C3−C4 bond in 1-hexene is weakest, and this is reflected in the lower heat of reaction of reaction 2 compared to the other C−C fission channels (reactions XI, 3, and XII).

In addition to these homolytic channels, 1-hexene may also dissociate via the retro-ene (1, 5 H-atom shift) pathway, producing two propenes:

$$1\text{-}C_6H_{12} \rightarrow CH_3CH{=}CH_2 + CH_3CH{=}CH_2 \qquad \Delta H_f^{298K} = 19.74 \text{ kcal/mol} \quad \text{(X)}$$

As confirmed by Tsang,[12] channel 2 is the dominant channel for 1-hexene dissociation. Channel XIII is neglected on the basis of the high barrier as well as relatively low entropy of activation. The rate constant for channel 2 given by Tsang[12] is 3−70 times his rate for channel X in the temperature range 1000−2000 K.[12] Furthermore, our test simulations and theory calculations indicate that channel X will be insignificant for the present experimental conditions. This is considered at length later.

Channel XII is also neglected on the basis of its high reaction barrier. Channels XI and 3 pose a different problem as they may make a marginal contribution to the overall rate. An interesting feature of channel XI is its subsequent dissociation steps. The $^{\bullet}C_5H_9$ radicals will primarily dissociate into ethylene and allyl radical[35]

$$^{\bullet}C_5H_9 \rightarrow C_2H_4 + {}^{\bullet}C_3H_5 \qquad \text{(XIV)}$$

whereas $^{\bullet}n$-C_3H_7 formed in reaction 2 mainly dissociates to C_2H_4 and CH_3 through[36]

$$^{\bullet}n\text{-}C_3H_7 \rightarrow C_2H_4 + {}^{\bullet}CH_3 \quad \Delta H_f^{298K} = 23.42 \text{ kcal/mol} \qquad (4)$$

As a result, channel XI forms essentially the same products as channel 2, and its likely small contribution is indistinguishable in the present modeling.

A rough estimate of the rate of reaction 3 was made assuming equal rates for the reverse recombination reactions. Then the ratio of rates for reaction 3 to reaction 2 is simply the equilibrium constant for

$$^{\bullet}C_3H_7 + {}^{\bullet}C_3H_5 \rightarrow {}^{\bullet}C_4H_7 + {}^{\bullet}C_2H_5 \qquad \text{(XV)}$$

Thus

$$k_\infty(3) \approx k_\infty(2)\, K_{eq}(\text{XV})$$

where

$$K_{eq}(\text{XV}) = 2.5 \exp\left(\frac{-11.8 \text{ kcal/mol}}{RT}\right)^{32}$$

This estimate for reaction 3 was introduced into the 1-hexene dissociation mechanism. As K_{eq}(XV) is much less than 1 in the given temperature range, the contribution of channel 3 will be minor compared to that of channel 2. It was found that, even at the highest experimental temperatures used for 1-hexene dissociation (∼1700 K), the contribution of channel 3 to the overall density gradient is less than 10%. Note that the rate used here for channel 3 is in compliance with the general observation discussed by Just:[37] Comparing two competitive dissociation channels, the relative contribution from the channel having the higher barrier starts diminishing as falloff increases.

From the above, channel 2 is considered the primary dissociation channel, and the reaction mechanism for 1-hexene dissociation was designed accordingly. The aforementioned channel 3 was nonetheless included as part of an estimated correction for the contributions to 1-hexene dissociation from channels other than channel 2.

1-Hexene Dissociation Mechanism. The mechanism for 1-hexene decomposition is now essentially reaction 2 and the subsequent decomposition of $^{\bullet}C_3H_7$ and $^{\bullet}C_3H_5$ radicals. Where available, rate constants for these decompositions were taken from the literature, especially those in refs 38−41. Falloff in unimolecular processes was calculated using RRKM theory wherever possible, and where not, available k_∞ values were reduced appropriately for falloff. The procedure used for RRKM rate constant estimation is straightforward; TST parameters (vibrational frequencies, rotational constants, and reaction barriers) were selected from the literature or calculated using electronic structure theory (G3B3),[42,43] with barriers adjusted when necessary to produce well-established k_∞ values. Falloff was then introduced in the reactions using recommended values[36,44] for $\langle\Delta E\rangle_{down}$. Some of the resulting estimated rate constants are discussed below.

C_3H_7 Dissociation. 1-Hexene primarily dissociates into *n*-propyl and allyl radicals via channel 2. The *n*-propyl radicals formed rapidly dissociate through two channels:

$$^{\bullet}n\text{-}C_3H_7 \rightarrow C_2H_4 + {}^{\bullet}CH_3 \quad \Delta H_f^{298K} = 23.42 \text{ kcal/mol} \qquad (4)$$

$$^{\bullet}n\text{-}C_3H_7 \rightarrow C_3H_6 + H \quad \Delta H_f^{298K} = 32.72 \text{ kcal/mol} \qquad (5)$$

For RRKM modeling of channel 4, B3LYP/6-31G(d) level frequencies scaled by 0.96 were used, with rotational constants and the reaction barrier taken from ref 45, whereas, for channel 5, all the parameters are from ref 36. For both channels, the selected RRKM model reproduced the recent evaluation of k_∞ by Curran.[46] For falloff corrections, a constant $\langle\Delta E\rangle_{down} = 500$ cm^{-1} was used for both channels on the basis of the discussion in ref 36.

C_2H_6 Decomposition. Ethane dissociation was studied by Kiefer et al.[47] over 1400−2200 K and 70−5700 Torr. The derived mechanism has also successfully predicted methyl radical recombination in acetaldehyde,[48] acetone,[49] methyl iodide,[50] and diacetyl[51] decomposition. Hence, the complete ethane mechanism (reactions 10−22, Supporting Information) of ref 47 is included here without modification. However, the F_{cent} parameter reported in ref 47 is in error, so the following corrected F_{cent} fit was used:

$$F_{cent} = (5.41867 \times 10^{-7})T^2 - (1.83149 \times 10^{-3})T + 1.78729$$

The above F_{cent} expression reproduces the theory rate constants in ref 47 within 4%.

C_3H_5 Dissociation. Fall off rate constants for allyl radical dissociation

$$^{\bullet}C_3H_5 \rightarrow C_3H_4 + H \quad \Delta H_f^{298K} = 56.71 \text{ kcal/mol} \qquad (6)$$

were obtained from the RRKM rate parameters reported by Fernandes et al.[52]

C_4H_8 Dissociation/Recombination. 1-Butene is of some importance in the mechanism because it is formed through the highly exothermic recombination of the prevalent $^{\bullet}C_3H_5$ and $^{\bullet}CH_3$ radicals. As can be seen from channels 2 and 4,

TABLE 1: RRKM Parameters for Reaction 7, $C_4H_8 \rightarrow {}^{\bullet}C_3H_5 + {}^{\bullet}CH_3$ (Gorin Model)

frequencies (B3LYP/6-31G(d)-scaled[53])	
C_4H_8 (30)	3104, 3030, 3009, 2997, 2989, 2948, 2925, 2901, 1665, 1476, 1467, 1451, 1418, 1379, 1310, 1279, 1253, 1163, 1061, 1000, 987, 957, 901, 830, 771, 628, 416, 303, 227, 105
TS (${}^{\bullet}C_3H_5 + {}^{\bullet}CH_3$) (24)	3132, 3046, 3024, 1483, 1233, 1005, 409, 742, 532, 977, 765, 514, 3130, 3039, 1474, 1382, 1174, 905, 3018, 435, 3186, 1374, 3186, 1374
moments of inertia (B3LYP/6-31G(d)[53]) (degeneracies in parentheses)	
molecular active	3.71×10^{-39} (1), 2.04×10^{-38} (1)
transition-state active	1.53×10^{-39} (1), 8.16×10^{-39} (1), 9.69×10^{-39} (1), 2.94×10^{-40} (1), 2.94×10^{-40} (1), 5.89×10^{-40} (1)
restriction parameter (η)	1−0.057
molecular mass	Kr, 83.80 amu; C_4H_8, 56.106 amu
Lennard-Jones parameters	$\sigma(C_4H_8) = 4.687$ Å, $\varepsilon/k_B(C_4H_8) = 531.4$ K (parameters for butane) $\sigma(Kr) = 3.655$ Å, $\varepsilon/k_B(Kr) = 178.9$ K
no. of Morse oscillators	1
E_A	76.10 kcal/mol
$\langle\Delta E\rangle_{down}$	$250\ (T/298)^{0.9}$cm^{-1}

virtually every reacting molecule of 1-hexene produces ${}^{\bullet}C_3H_5$ and ${}^{\bullet}CH_3$. Hence, a fast rate of this exothermic recombination reaction can make a significant contribution to the overall gradient.

This recombination is introduced in the mechanism through its reverse, 1-butene dissociation

$$1\text{-}C_4H_8 \rightarrow {}^{\bullet}C_3H_5 + {}^{\bullet}CH_3 \quad \Delta H_f^{298K} = 76.05 \text{ kcal/mol} \tag{7}$$

For the RRKM model of this C−C bond fission reaction, a restricted-rotor Gorin model appropriate to the loose transition state was employed. Frequencies and moments of inertia of C_4H_8 and the TS (${}^{\bullet}C_3H_5 + {}^{\bullet}CH_3$), calculated at the B3LYP/6-31G(d) level of theory, were taken from ref 53. The Gorin restriction parameter and reaction barrier were then modified to match the k_∞ given by Dean.[54] Then the standard form of $\langle\Delta E\rangle_{down}$ suggested by Miller and Klippenstein[44] was used for falloff. The RRKM−Gorin parameters for reaction 7 are compiled in Table 1.

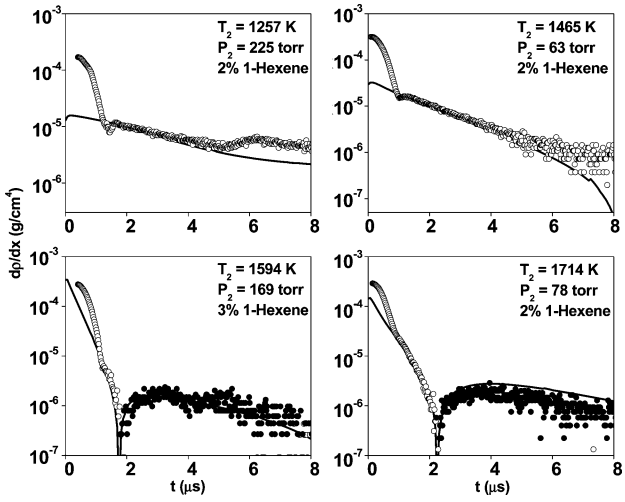

Figure 1. Semilog absolute density gradient profiles showing 1-hexene dissociation in 1-hexene/Kr mixtures at the indicated temperature, pressure, and composition. Empty and filled circles represent positive and negative experimental density gradients, respectively. Solid lines are simulations generated with the recommended 1-hexene dissociation mechanism.

1-Hexene Experiments. Figure 1 shows four representative LS dissociation experiments in 1-hexene at different temperatures, pressures, and reactant mole fractions. These semilog plots show absolute values of $d\rho/dx$, and empty and filled circles represent positive and negative $d\rho/dx$, respectively. The solid lines in these figures are simulations generated with the full 1-hexene dissociation mechanism (reactions 2−74, Supporting Information). All the 1-hexene experimental profiles were fit only adjusting the rate of reaction 2 while keeping all the other reaction rates in the mechanism fixed at their initial estimates. To recognize falloff effects in the various unimolecular reactions in this model, different rates were used for the 50 and 200 Torr experiments. The initial positive gradients are dominated by the endothermic dissociation reaction (channel 2), whereas the late time negative gradients at high pressures are produced by exothermic recombination of methyl radicals, forming ethane (−10), as well as the combination of CH_3 and H-atoms with stable allyl radicals, producing propene (−35) and 1-butene. Note that the model is able to properly predict the magnitude of positive and negative density gradients and the onset of negative gradients. The derived bond fission rate constants for 1-hexene dissociation are displayed in the Arrhenius plot of Figure 2.

For the simple C−C bond fission reaction (channel 2), a restricted-rotor Gorin RRKM model of a loose transition state was used. The model is delineated in Table 2. The $\langle\Delta E\rangle_{down}$ and the restriction parameter (η) in the model were selected so that, within experimental error, the model closely predicted the characteristics of the experimental rates. The resulting

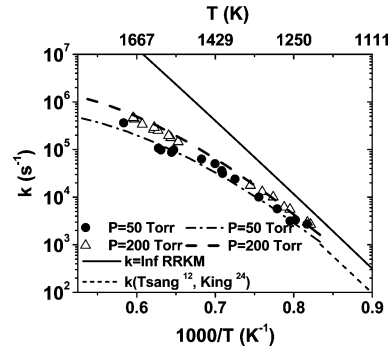

Figure 2. Arrhenius plot of laser-schlieren rate constants for 1-hexene dissociation (reaction 2).

TABLE 2: RRKM Parameters for Reaction 2 (1-C_6H_{12} → $^{\bullet}C_3H_5$ + $^{\bullet}C_3H_7$ (Gorin Model)

frequencies (at B3LYP/6-311+G(3df,2p); scaling factors used are 1.01 for low frequencies and 0.9679 for high frequencies[55])	
C_6H_{12}	74.9, 92.2, 129.1, 177.6, 244.7, 344.5, 346, 444, 632, 712.7, 773.5, 869, 897.4, 909., 922.1, 983.4, 998.5, 1017.9, 1023.1, 1087, 1158.8, 1207.7, 1235.9, 1269.6, 1282.1, 1291.8, 1311.8, 1345.2, 1369.7, 1410.3, 1436, 1442.4, 1452.5, 1453.5, 1465, 1647.8, 2891.5, 2899.6, 2907.8, 2918.8, 2920.2, 2932.9, 2951.3, 2976.8, 2981.1, 3009, 3023.3, 3101.1
$^{\bullet}C_3H_5$	416.6, 514.5, 534.5, 774.7, 799.3, 909.5, 983.5, 1005.7, 1170.1, 1233.7, 1381.7, 1466, 1472.8, 3025.9, 3033.4, 3039.1, 3127, 3129.4
$^{\bullet}C_3H_7$	33.5, 250.6, 329.9, 531.9, 725.2, 861.9, 866, 984.5, 1058.6, 1157.3, 1267.2, 1280.6, 1354.6, 1421.9, 1440.5, 1447.9, 1459.4, 2906.2, 2921.8, 2937.4, 2983.2, 2991.8, 3030.7, 3125.9
moments of inertia (degeneracies in parentheses)	
molecular active (estimated)	6.75×10^{-38} (1), 6.88×10^{-38} (1)
transition-state active (estimated)	1.52×10^{-39} (1), 8.08×10^{-39} (1), 9.60×10^{-39} (1), 2.66×10^{-39} (1), 9.50×10^{-39} (1), 1.06×10^{-38} (1)
transition-state restriction parameter (η)	0.95
molecular mass	Kr, 83.80 amu; 1-hexene, 84.16 amu
Lennard-Jones parameters	σ(1-hexene) = 5.949 Å, ε/k_B = 399.3 K
	σ(Kr) = 3.655 Å, ε/k_B = 178.9 K
no. of Morse oscillators	1
E_0 (ΔH_{0K})	73.74 kcal/mol (G3B3)
$\langle\Delta E\rangle_{down}$	640 cm^{-1}

high-pressure-limit rate constant for reaction 2 from the RRKM model fit is

$$k_\infty(2) = (1.464 \times 10^{27})T^{-3.03} \exp((-78.55 \text{ kcal/mol})/RT) \text{ s}^{-1} \quad (T = 1200-1700 \text{ K}, <0.1\ \% \text{ error})$$

or in Arrhenius form

$$k_\infty(2) = (1.46 \times 10^{16}) \exp((-69.12 \text{ kcal/mol})/RT) \text{ s}^{-1} \quad (T = 1200-1700 \text{ K}, <7\ \% \text{ error})$$

This is 3−4 times higher than the k_∞ of Tsang.[12] This difference is discussed later in the text.

A problem exists with the entropy of 1-hexene, caused by its numerous low-barrier internal rotations. The properties used herein (entropy and heat capacity) were obtained from group additivity.[32] This should deal with this internal rotation problem adequately if indirectly. In fact, reasonable estimates for the 1-hexene partition function can also be obtained from these estimates. On the other hand, an RRKM calculation requires an additional explicit hindered rotor treatment of torsional modes in the transition state, and this is beyond present group-additivity estimation. For these RRKM calculations, any necessary correction for these hindered rotations is considered to be effectively included by adjustment of the restriction parameter (η). This restriction parameter not only corrects for the restriction of internal rotation in the TS on bringing together infinitely separated product fragments, but also should deal with flaws in the treatment of hindered rotation in the partition functions of the reactant and the transition state.

The laser-schlieren data presented here clearly demonstrate that any contribution from the retro-ene channel, reaction X, like other molecular product channels, must be minor. This is seen when a few low-temperature experiments are modeled using reaction X as the only 1-hexene dissociation channel. Here the rate constant for reaction X was chosen as the k_∞ reported by Tsang,[12] and the secondary mechanism is again that given in the Supporting Information. Here density gradients obtained from reaction X were 2 orders of magnitude lower than the experimental density gradients, a consequence of both the low endothermicity of reaction X and the stability of the propene product. Thus, the laser-schlieren experiments exclude any large contribution from this reaction.

Cyclohexane. ***Relaxation.*** In large molecules without very low vibrational frequencies such as cyclohexane, it is often possible to observe relaxation and even unimolecular incubation.[31,56] Some low-pressure and low-temperature experiments were able to resolve the relaxation, but the process was found to be very fast and could only be resolved at the lowest pressures where dissociation gradients are negligible. Hence, it was not possible to observe the unimolecular incubation in cyclohexane. To examine relaxation, 10 extremely low pressure experiments were performed. Examples with pure relaxation gradients—raw signals and resulting semilog plots—are shown in Figure 3.

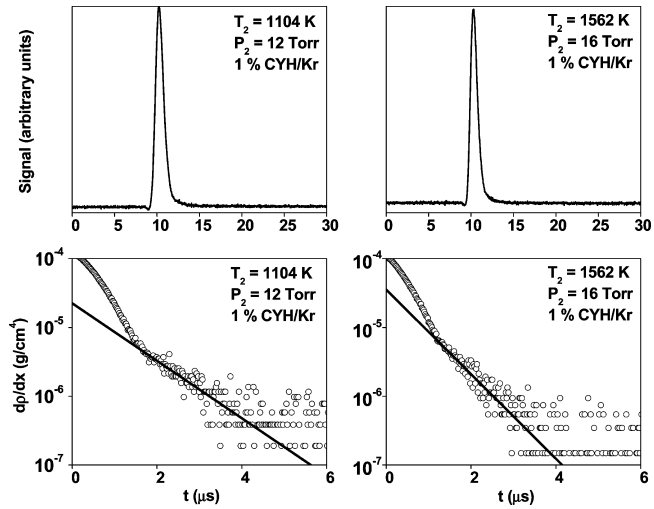

Figure 3. Raw profiles and semilog plots of laser-schlieren gradients for pure relaxation in cyclohexane/Kr mixtures. In these semilog plots, the first few rapidly falling early points arise from beam−shock front interaction, i.e., the initial schlieren spike in the raw profiles (top row). The small curve following the initial spike in the raw-data plots is relaxation.

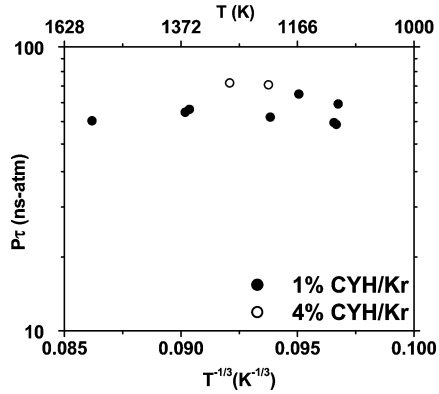

Figure 4. Landau−Teller plot of vibrational relaxation times for cyclohexane/Kr mixtures.

As expected, relaxation this fast is closely exponential. Results for the energy relaxation time, τ, as defined through the Bethe−Teller relation,[30,57] are shown in Figure 4. The procedure used for extraction of the relaxation time is explained in refs 29 and 30.

In Figure 4 it is seen that, for 1100−1500 K, vibrational relaxation in cyclohexane is indeed extremely fast and nearly temperature independent. Contrary to expectations,[56] relaxation times for the 4% cyclohexane/Kr experiments seem a bit longer than those for the 1% experiments, but this small discrepancy may simply be experimental error for such fast relaxation and is considered insignificant.

Incubation time measurements require the presence of a well-resolved relaxation clearly followed by unambiguous dissociation in the same experiment. Again, in cyclohexane, the low pressures required to observe relaxation obviate incubation measurements since dissociation gradients are then too weak to discern. To estimate incubation times, ratios of incubation time to relaxation time (t_i/τ) for the similarly sized molecule neopentane[30] were used. The neopentane t_i/τ measurements were fitted to an Arrhenius form to within 13% error:

$$t_i/\tau = 0.075 \exp(6000/T)$$

In the 1100−1550 K temperature range, cyclohexane relaxation shows no discernible temperature dependence, and hence, a constant relaxation time $\tau = 62$ ns atm was used for the entire temperature range of dissociation.

Using the above equation, incubation times were calculated for all pressure ranges. The 100, 150, and 200 Torr experiments now had incubation times of ≤ 0.2 μs, and such small time shifts were neglected because uncertainties associated with the location of the time origin[58] are expected to be as large as these.[59] Small incubation delays were, however, introduced in the modeling of the 25 Torr experiments. However, the 50 Torr experiments were not significantly affected by incubation, and incubation delays were not introduced in these experiments. This neglect is again discussed below.

Possible Dissociation Channels. An energy diagram for cyclohexane is presented in Figure 5, constructed using $\Delta H_f^\circ{}_{298K}$ and $H_{298} - H_0$ from Burcat and Ruscic.[19] Energies of the given transition states were taken from new calculations and the literature.[23] When a dissociation channel proceeds through a diradical, more than one step will be involved, e.g., channel 1 is here reaction Ia followed by reaction Ib. In such cases, only the rate-controlling transition states (highest energy TS) are shown on the energy diagram. Transition states TS1, TS4, and

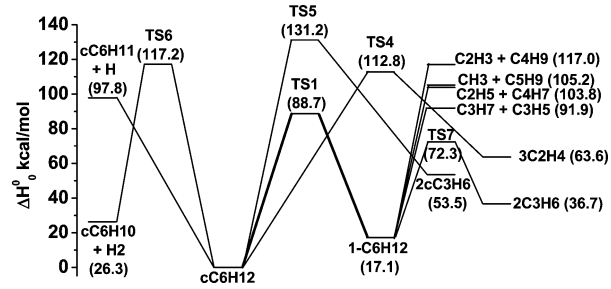

Figure 5. Energy diagram depicting possible cyclohexane/1-hexene dissociation channels having species and TS energies relative to cyclohexane.

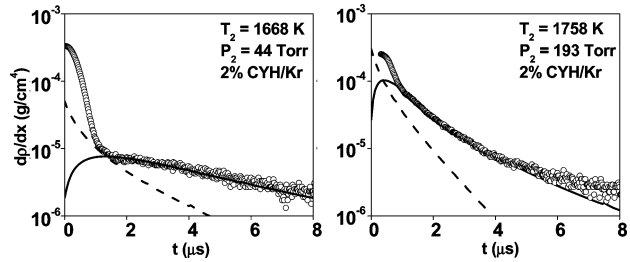

Figure 6. Comparison between density gradients generated by the two possible channels 1 and II. The solid line uses only channel 1 for the cyclohexane dissociation channel, but includes the mechanism for the dissociation of the 1-hexene product, whereas the dotted line is generated using channel II and the ethene dissociation as the sole cyclohexane reactions.

TS5 are thus rate-controlling for channels 1 and II and the other molecular channel c-$C_6H_{12} \rightarrow$ 2 c-C_3H_6,[23] which in fact are the transition states of elementary reactions Ia, IIaa, and IX, respectively. The energy for TS1 is from CASPT2/cc-pVDZ calculations, whereas the energies of TS4 and TS5 are taken from ref 23. $\Delta H_f^\circ{}_{298K}$ and $H_{298} - H_0$ for the $^\bullet C_5H_9$ radical and the energies of TS6 and TS7 were calculated using molecular parameters from the G3B3 level of theory.

We have estimated a k_∞ for the C−H fission reaction (channel V) assuming the rate of the reverse H + c-$C_6H_{11} \rightarrow$ c-C_6H_{12} is the same as that of the reaction H + iso-$C_3H_7 \rightarrow C_3H_8$ taken from ref 60, with the result $k_\infty(V) = (6.8 \times 10^{15}) \exp(-97.0/RT)$. This is then not competitive and has thus been ignored in the modeling.

The result is channel 1 is the lowest energy channel among all the possible channels for cyclohexane dissociation and is thus expected to be the dominant channel. As illustrated in the example attempt to model the experiments of Figure 6 with reaction II, the gradient observed in the LS experiments cannot be described with a major contribution from any of the molecular channels II, III, IV, or VI. This is simply because the endothermicity resulting from these is small and ultimately not adequate at any time as the products are also quite stable and do not themselves react. Thus, theory and experiment are in full accord on the dominance of reaction 1 as the initial step in cyclohexane decomposition. None of the proposed molecular channels make a significant contribution to the overall dissociation rate, even for the highest temperatures used herein. Having all the decomposition through channel 1 alone is also supported by the previous experimental work of both Tsang[12] and Brown et al.[15]

Cyclohexane Experiments. In the low-temperature experiments shown in Figure 7, the "two-step" process of reaction 1 followed by reaction 2, with further reactions of the 1-hexene decomposition, is seen to produce the fully resolved upward

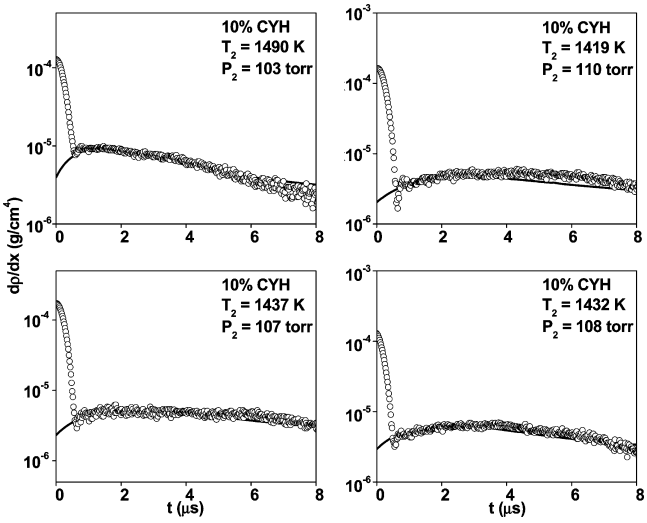

Figure 7. Semilog plots of curved density gradient profiles produced by pyrolysis of cyclohexane/Kr mixtures at the indicated temperatures and pressures. The open circles are the measurements, and the solid lines in these figures are simulations generated by the two-step process of reactions 1 and 2.

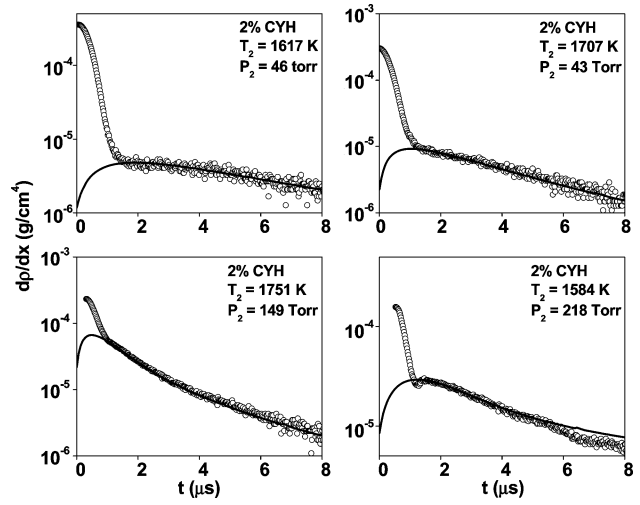

Figure 8. Semilog density gradient profiles showing cyclohexane dissociation in cyclohexane/Kr mixtures for the indicated temperature, pressure, and composition, having partially resolved maxima. The open circles are the measurements (positive density gradient), and the solid lines in these figures are simulations generated with the two-step process. The secondary reaction mechanism given in the Supporting Information is used with reactions 1 and 2.

curvature in these experiments, and this curvature is quite unambiguous evidence for this two-step process.

The above curvature is a consequence of the small endothermicity of the initial cyclohexane isomerization (reaction 1), just 19 kcal/mol, whereas the endothermicity of the product 1-hexene dissociation through the faster reaction 2 is 75 kcal/mol. The further decomposition of its allyl and *n*-propyl products now increases this even more. Of course, at $t = 0$, only the cyclohexane isomerization contributes to the density gradient. The small gradient generated by this then rises strongly as 1-hexene is formed and rapidly dissociates. After a short time, the density gradient reaches a maximum which roughly corresponds to a steady state in the 1-hexene. Beyond this the gradient falls, as usual, from temperature drop and depletion. Some of the higher temperature experiments shown in Figure 8 also appear to capture indications of the resulting curvature.

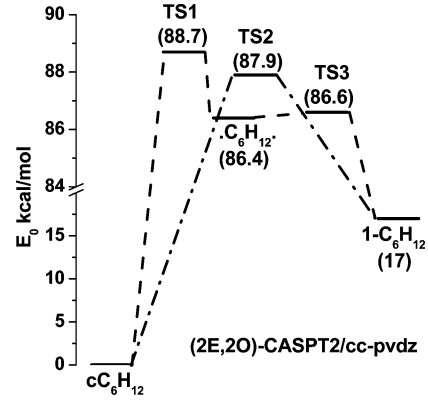

Figure 9. Potential energy diagram for cyclohexane isomerization/dissociation calculated at the CASPT2/cc-pVDZ level. Note the break in the *y* axis. TS1 is a transition state for the cyclohexane ring-opening to a diradical, whereas TS2 is the transition state for isomerization to 1-hexene through a single elementary step. TS3 is the transition state for diradical isomerization to 1-hexene.

The potential energy surface (PES) for cyclohexane isomerization was separately studied in detail at the CASPT2/cc-pVDZ level of theory. These calculations show that the diradical isomerizes to 1-hexene. Energies obtained for isomerization channels 1, Ia, and Ib are shown on Figure 9. An interesting feature of these calculations is the transition state TS2, which represents isomerization of cyclohexane to 1-hexene through a single step avoiding formation of the diradical intermediate. Although the barrier to TS2 is a bit lower than the ring-opening barrier TS1, this elementary step is not favored because of its lower entropy of activation. We estimate that this process contributes no more than 10% of the total reaction rate.

We again conclude, on the basis of Figures 7 and 8, and the above PES study, that 1-hexene is the only significant product of the initial reaction. The 1-hexene dissociation mechanism was accordingly included unchanged in the cyclohexane dissociation calculations presented in these figures, where the combination produces an excellent fit to the experiments. RRKM-derived rate constants for reaction 2 (Table 2 and Figure 2) at the various pressures were used in this modeling. Also, falloff effects were recognized in the secondary unimolecular reactions, as described earlier. Other reactions exclusive to the cyclohexane decomposition are described below. It was observed that H-atom abstraction from 1-hexene did not have a significant effect on the consumption of 1-hexene given its fast dissociation. Cyclohexane dissociation, on the other hand, is much slower, and H-atom abstraction reactions may have a considerable effect on the consumption of cyclohexane by radicals present in the reaction mixture. One additional point: the equilibrium constant for reaction 1 is $O(100)$ here, and because the 1-hexene is also less stable, reaction 1 does not back up for the present conditions.

Figure 10 shows a comparison between the various H abstraction channels from cyclohexane by H, CH_3, C_2H_3, C_3H_5, and C_2H_5 radicals. As seen, H-atoms from cyclohexane are mainly abstracted by H and CH_3 radicals, reactions 75 and 76. *[Note again that these reactions are numbered according to their numbering in the full mechanism given in the Supporting Information*]. Other radicals such as C_2H_3, C_3H_5, and C_2H_5 also abstract, but were not included given low radical concentrations and lower abstraction rate constants in comparison with those of abstraction by H and CH_3 radicals.

$$H + c\text{-}C_6H_{12} \rightarrow {}^{\bullet}c\text{-}C_6H_{11} + H_2 \quad (75)$$

$$^{\bullet}CH_3 + c\text{-}C_6H_{12} \rightarrow {}^{\bullet}c\text{-}C_6H_{11} + CH_4 \quad (76)$$

The rate constant for reaction 75 was determined theoretically. Geometries, vibrational frequencies, and rotational constants were calculated at the B3LYP/6-311++G** level of theory. The potential was calculated with the G2-like method RQCISD(T)/6-311++G** + RMP2(full)/6-311++G(3df,2pd) − RMP2/6-311++G**. A transition-state-theory rate with Eckhart tunneling correction was then calculated for the boat and chair conformers, and a thermal average of rates for the equilibrium mixture was obtained. The rate constant for reaction 76 and the other rates in Figure 10 were estimated using the known rate constant for H-atom abstraction from the $-CH_2-$ group of propane, multiplied by 6 for the six secondary carbon atoms in cyclohexane. Subsequent H-atom abstractions from cyclohexyl radical were not included because of its low stability and low concentration. Cyclohexyl radical decomposition was treated using rates from ref 64. The final modeling of the cyclohexane dissociation experiments included the unmodified mechanism for 1-hexene. All the profiles are modeled by adjusting only the rate of reaction 1 (or reaction 1A, see below, for the 25 Torr experiments).

As discussed earlier, incubation delays were included only for the 25 Torr experiments. To include falloff, different mechanisms were used for modeling the 25, 50, 100, 150, and 200 Torr experiments. Additional example laser-schlieren profiles for cyclohexane dissociation are shown in Figure 11, examples which serve to complete the range of the experiments. Again, the two-step model whose results are shown here as the solid lines, is the standard model where reaction 1 is followed by reaction 2, here contrasted with the "one-step" model of reaction 1A, discussed below, whose predictions are shown by the dotted lines in Figure 11. These two models are described in detail in the next section.

As can be seen in Figures 1 and 11, low-temperature cyclohexane dissociation experiments exhibit large density gradients even at late times, whereas, in the highest temperature experiments, the gradient is reduced to the order of 10^{-6} g/cm^4 (order of noise in the laser-schlieren experiments) after just 4 μs. One interesting feature of the density gradient for cyclohexane dissociation is the presence of only very weak negative gradients compared with 1-hexene dissociation, even though

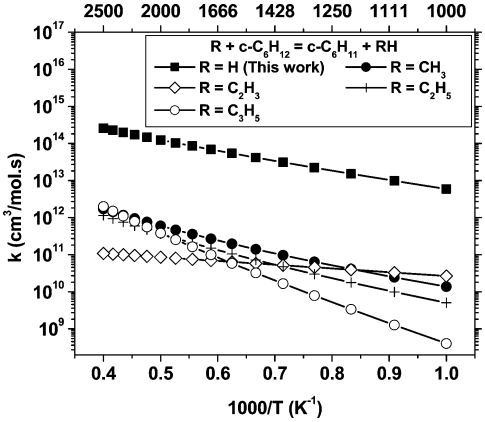

Figure 10. Rate constants for H-atom abstraction from cyclohexane by R = H, $^{\bullet}CH_3$, $^{\bullet}C_2H_3$, $^{\bullet}C_3H_5$, and $^{\bullet}C_2H_5$ radicals: (i) R = H, present work; (ii) R = $^{\bullet}CH_3$, estimated;[61] (vi) R = $^{\bullet}C_2H_3$, estimated;[62] (vii) R = $^{\bullet}C_2H_5$, estimated;[61] (viii) R = $^{\bullet}C_3H_5$, estimated.[63]

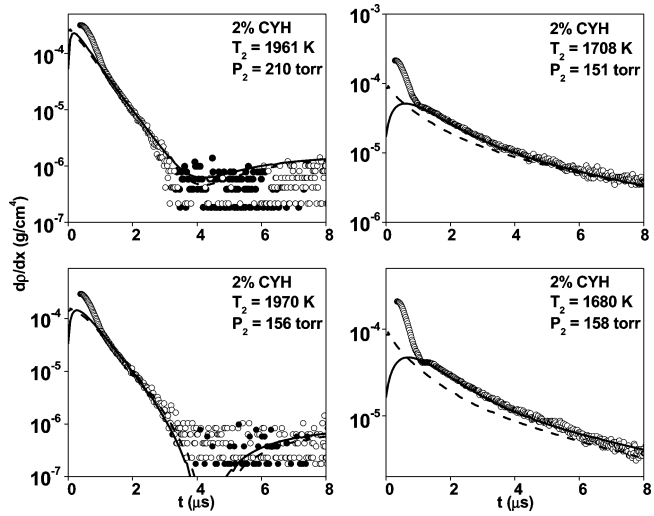

Figure 11. Semilog density gradient profiles showing cyclohexane dissociation in cyclohexane/Kr mixtures for the indicated temperature, pressure, and composition having essentially unresolved maxima. The solid and dotted lines in these figures are simulations generated with the two-step and the one-step processes, respectively.

both ultimately turn on the same 1-hexene reactions. In 1-hexene dissociation the late exothermicity responsible for this arises mainly from H and CH_3 combination with C_3H_5 radicals, forming C_3H_6 and 1-C_4H_8, and from CH_3 recombination. These channels are mitigated in cyclohexane dissociation as the H and CH_3 radicals are significantly consumed by abstraction from the relatively stable and persistent cyclohexane, reactions 75 and 76.

Alternate One-Step Model. The cyclohexane energy diagram in Figure 5 suggests that the energies of TS1 and the C_3H_7 + C_3H_5 fission channel for 1-hexene are very close. It is then entirely possible that, for low pressures (lower rate of collisional deactivation) and/or high temperatures (higher excitation energies), cyclohexane will dissociate via the one-step reaction

$$c\text{-}C_6H_{12} \rightarrow {}^{\bullet}C_3H_7 + {}^{\bullet}C_3H_5 \quad (1A)$$

with chemically activated 1-hexene directly producing C_3H_7 and C_3H_5 radicals. Then the stabilized intermediate 1-hexene is missing, and the previous maxima in the gradient will no longer appear. This one-step process will of course produce the same products as the previous two-step process of reaction 1 followed by reaction 2, but the one-step process does not involve the isomerization and must therefore lack the curvature clearly shown in Figure 7.

Although there is no evidence for the above in the modeling of any of the experiments considered thus far, the few extremely low-pressure (~25 Torr), high-temperature experiments shown in Figure 12 may yet indicate a dominance of the one-step process. Unfortunately, because of their extremely low pressures, these experiments present unique problems. Inasmuch as the relaxation in cyclohexane is fast, but not instantaneous, it is necessary to recognize the possibility of incubation delays in the modeling. In the examples of Figure 12, the flat gradients generated by the one-step model (reaction 1A) provide a slightly superior fit when incubation delay is recognized. Recognizing this as the more likely situation, all the 25 Torr experiments were modeled using reaction 1A instead of reaction 1 as the cyclohexane dissociation channel. However, it is noted that the rate constants required for reactions 1 and 1A then differ only

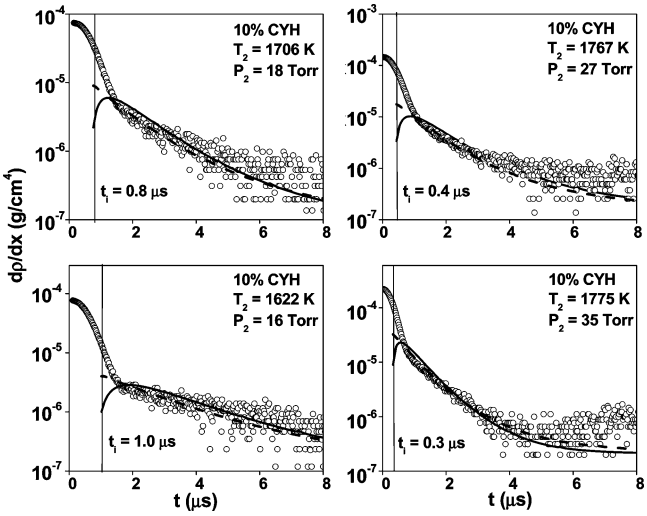

Figure 12. Semilog plots of density gradient profiles produced by pyrolysis of cyclohexane/Kr mixtures at the indicated high temperatures and very low pressures. The solid and dotted lines in these figures are simulations generated with two-step and one-step processes, respectively (see the text).

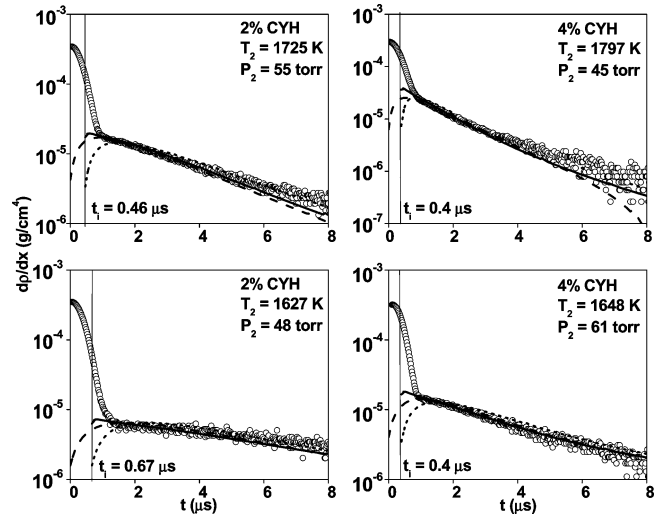

Figure 13. Semilog density gradient profiles showing cyclohexane dissociation in cyclohexane/Kr mixtures for the indicated temperatures, pressures, and compositions. The simulations in these figures are generated with the one-step process (reaction 1A) with incubation delay (solid line), the two-step process (reactions 1 and 2) with incubation delay (dotted line), and the two-step process without incubation delay (dashed line).

by 20%, about the expected experimental uncertainty in the laser-schlieren experiments, and hence, the choice of model does not much affect the derived initiation rate constants.

In the two higher pressure and lower temperature experiments of Figure 11, the pair on the right of the figure, only the two-step model can describe the curved density gradient profile. As demonstrated, the one-step scheme fails to model the experimental profiles in this case even when the simulations are shifted by estimated incubation delays ($t_i < 0.2$ μs), whereas the high-temperature experiments in Figure 11 can be modeled using either process because here the initial rise to the maximum is too short to affect the result.

The intrusion of the one-step process remains uncertain for intermediate-pressure (~50 Torr) experiments. At such pressures, incubation times based on the neopentane study do predict delays greater than 0.2 μs, and their effect on the dissociation rate constants should be investigated. It was demonstrated in the ~150 Torr experiments of Figure 11 that the density gradients predicted by the one-step model were too low to fit large initial experimental density gradients, but now in the 50 Torr experiments, the incubation delays may compensate for low one-step gradients, and the experimental data can be successfully simulated. The possible effects of such incubation delays on these experiments are considered here.

Figure 13 shows four 50 Torr experiments modeled with three possible schemes, a one-step process (reaction 1A) with estimated incubation delay, a two-step process with this incubation delay, and a two-step process without incubation delay. The rate constants for cyclohexane dissociation (channel 1 or 1A) were again adjusted separately in each to obtain the closest fit keeping the rest of the mechanism fixed.

In Figure 13 it is evident that the 50 Torr experiments are actually very well modeled by the two-step model when no incubation delay is introduced, whereas, when incubation delays are included, the one-step model seems to perform somewhat better. This is especially evident from the 1648 and 1725 K experiments in Figure 13, where the solid lines (one-step model plus incubation delay) capture the entire experimental gradient, whereas the dotted lines (two-step model plus incubation delay) miss the important initial gradient following the schlieren spike. This might seem to be evidence of the one-step process in

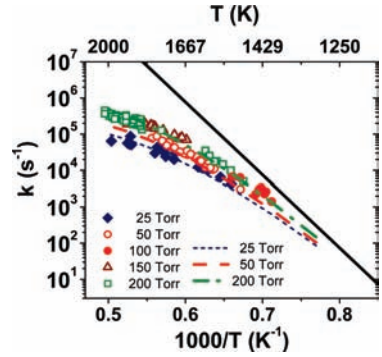

Figure 14. Arrhenius plot of rate constants for cyclohexane isomerization to 1-hexene (reaction 1).

cyclohexane dissociation, but one cannot be certain because of the considerable uncertainty in the estimated incubation times. In a way this ambiguity in the dissociation step is, however, again not serious; the rate constants for cyclohexane dissociation (channel 1 or 1A) used for all three models differ by less than 20%.

The derived rate constants for cyclohexane dissociation from all the fitted experiments are displayed on the Arrhenius plot of Figure 14. Each displayed rate constant is obtained from a match of a computed profile to the individual experiment, adjusting only the initiation rate. The lines on the plot are from slightly simplified RRKM calculations. An accurate RRKM treatment for predicting falloff in the cyclohexane dissociation is complicated by a number of factors. For one thing, the diradical and molecule have several conformational forms which need to be considered separately, and singlet and triplet states of the diradical may pose additional difficulty. The two electronic states are almost identical in energy with the well-separated radical sites in the diradical, and unlike the singlet diradical, the triplet cannot recombine. Thus, it was decided to use the RRKM calculations to merely provide an appropriate means of extrapolation to an experimental k_∞. The ring-opening of cyclohexane was considered to be the sole rate-controlling step, and the direct isomerization indicated in Figure 9 was

TABLE 3: RRKM Parameters for Reaction Ia, c-C_6H_{12} → $^{\bullet}C_6H_{12}{}^{\bullet}$ (Vibrational Model)

frequencies (B3LYP/CBSB7 (scale factor 0.99)[23])	
c-C_6H_{12} chair (48)	225.1, 225.1, 371.4, 422.8, 422.8, 516.0, 782.7, 782.8, 792.7, 854.7, 854.7, 906.9, 906.9, 1025.8, 1025.8, 1031.2, 1063.8, 1084.4, 1119.8, 1167.9, 1273.4, 1273.4, 1279.6, 1279.6, 1336.0, 1358.0, 1364.7, 1364.7, 1370.9, 1370.9, 1469.7, 1469.7, 1474.9, 1474.9, 1480.8, 1495.7, 2965.5, 2965.5, 2966.7, 2973.8, 2973.8, 2978.0, 3018.2, 3018.2, 3019.6, 3019.6, 3022.6, 3027.1
TS (47)	95.2, 118.5, 129.8, 184.3, 235.3, 334.1, 383.8, 452.3, 496.5, 510.0, 753.6, 725.9, 803.2, 876.5, 887.3, 929.6, 1001.2, 1025.5, 1076.7, 1094.5, 1130.3, 1182.3, 1211.0, 1241.7, 1289.7, 1344.5, 1353.5, 1372.6, 1376.4, 1444.1, 1445.5, 1451.3, 1455.5, 1472.7, 1476.4, 2886.2, 2889.2, 2973.2, 2985.0, 2993.1, 3001.0, 3019.3, 3025.7, 3096.8, 3101.7, 3198.5, 3201.7
moments of inertia (B3LYP/CBSB7[23]) (degeneracies are in parentheses)	
molecular active	1.957×10^{-38} (1)
transition-state active	1.795×10^{-38} (1)
molecular inactive	1.957×10^{-38} (1), 3.434×10^{-38} (1)
transition-state inactive	3.375×10^{-38} (1), 4.300×10^{-38} (1)
molecular mass	Kr, 83.80 amu; C_6H_{12}, 84.16 amu
Lennard-Jones parameters	σ(c-C_6H_{12}) = 6.182 Å, ε/k_B(c-C_6H_{12}) = 297.1 K
	σ(Kr) = 3.655 Å, ε/k_B(Kr) = 178.9 K
no. of Morse oscillators	0
E_A	86.0 kcal/mol
$\langle\Delta E\rangle_{down}$	600 cm^{-1}

neglected. A vibration-model RRKM calculation, using a transition state for reaction Ia,

$$\text{c-}C_6H_{12} \rightarrow {}^{\bullet}C_6H_{12}{}^{\bullet} \qquad \text{(Ia)}$$

was then used for falloff calculations. For the molecule, the harmonic frequencies of the cyclohexane chair structure (no. 1 in the paper by Sirjean et al.[23]) and the transition state for reaction Ia (TS1 → TS3 of ref 23) were scaled by 0.99 as per the recommendation also given in ref 23. Moments of inertia of cyclohexane and the TS were also obtained from this with their lowest moments considered active and the remainder adiabatic.[65] The barriers for the ring-opening process from ref 23 and from our own CASPT2/cc-pVDZ level of theory were 88.8 and 88.7 kcal/mol, respectively. Calculations with these barriers and selected TS properties failed to fit the falloff at high temperatures, so the barrier was reduced to 86.0 kcal/mol in the model. Note that this does not really imply error in the cited calculations of the barrier; over the present temperature range an equivalently adequate fit could be obtained by simply increasing the magnitude of the calculated rates by about a factor of 2.5.

The vibrational RRKM model used here is detailed in Table 3. The $\langle\Delta E\rangle_{down}$ value was selected so that, within experimental error, the model predicted characteristics of the experimental falloff adequately. The $\langle\Delta E\rangle_{down}$ of 600 cm^{-1} used here is a common choice comparable to other $\langle\Delta E\rangle_{down}$ values used in the literature for similarly sized molecules.[66]

The resulting high-pressure-limit rate constant for reaction 1 from the RRKM model is

$$k_\infty(1) = (4.03 \times 10^{16})T^{0.367} \exp((-90.76 \text{ kcal/mol})/RT) \text{ s}^{-1}$$
$$(T = 1300-2000 \text{ K}, <0.1\% \text{ error})$$

and forcing the Arrhenius form

$$k_\infty(1) = (8.76 \times 10^{17}) \exp((-91.94 \text{ kcal/mol})/RT) \text{ s}^{-1}$$
$$(T = 1300-2000 \text{ K}, <1\% \text{ error})$$

Some of the various high-pressure rate constants for the cyclohexane isomerization are compared to the above results in Figure 15. As was the case with 1-hexene, the current rate is again 3−4 times higher than Tsang's k_∞, but agrees well with the expressions given by Brown et al.[15] and Sirjean et al.[23]

The disagreement with Tsang on the rate constants for both 1-hexene and cyclohexene needs further consideration. Tsang carried out his experiments in a single-pulse shock tube where the reacting mixture is cooled by synchronized rarefaction waves,[67] and he used 1-methylcyclohexene and cyclohexene as internal comparators for his cyclohexane and 1-hexene dissociation studies, respectively.[12] Use of cyclohexene as an internal standard for the cyclohexane experiments had to be avoided because 1,3-butadiene is also a product of cyclohexane decomposition.

A first issue concerns the formation of propene, mainly assigned by Tsang to the retro-ene reaction of the 1-hexene. The 1-hexene decomposition was carried out in an excess of toluene as a chain inhibitor (0.01% 1-hexene, 1% toluene in Ar). To estimate the rate of the retro-ene channel (reaction X), it seems all the propene formed was attributed to the retro-ene reaction (channel X) and reaction 5, the minor path in *n*-propyl decomposition,

but this ignores the likely formation of propene via H-atom abstraction by allyl radicals from the large quantity of toluene:

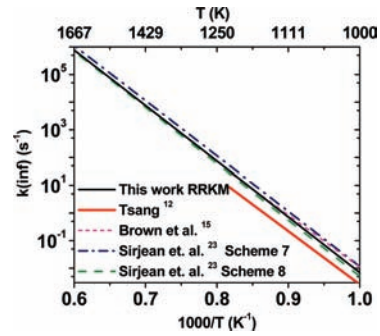

Figure 15. Comparison of the present and literature high-pressure-limit rate constants for cyclohexane dissociation.

$$^{\bullet}C_3H_7 \rightarrow C_3H_6 + H \quad (5)$$

$$^{\bullet}C_3H_5 + C_7H_8\ (\text{toluene}) \rightarrow C_3H_6 + {}^{\bullet}C_7H_7\ (\text{benzyl}) \quad (XVI)$$

$^{\bullet}C_3H_5$ will certainly dissociate into a-C_3H_4 and H

$$^{\bullet}C_3H_5 \rightarrow \text{a-}C_3H_4 + H \quad (6)$$

but the rate of reaction XVI (ref 68) is actually 18−2000 times faster than that of reaction 6 (ref 52) over Tsang's experimental range.[12] Ignoring reaction XVI in the formation of propene may then force an overestimate for the rate of channel X. Given the lack of well-defined literature rate coefficients for reaction XVI in our temperature range, this overestimation could not be quantified. However, a theoretical rate constant of (2.87×10^{12}) exp((−57.33 kcal/mol)/*RT*) s^{-1} for channel X, derived here from a G3B3 TST calculation,[42,43] is actually in good agreement with Tsang's rate constant. Thus, it seems that the neglect of reaction XVI by Tsang somehow does not much affect his rate constant for channel X.

The experimental pressures in Tsang's cyclohexane and 1-hexene experiments are 2−7 and 1.5−6 atm, respectively, but even for these high pressures, falloff in the reactions is not completely avoided. We have used our new RRKM models of Tables 2 and 3 to estimate falloff for Tsang's experimental conditions, and the results are shown in Figure 16.

In Figure 16, it is seen that falloff is more pronounced in 1-hexene than in cyclohexane; it is simply a faster reaction. As seen in the calculations of Figure 16 the extent of falloff in cyclohexane for Tsang's conditions is within experimental uncertainty. However, in 1-hexene, the RRKM falloff rate constants are 40% lower than the RRKM k_∞ and are now only a factor of 2 higher than Tsang's k_∞ values, whereas the RRKM k_∞ is 4 times higher than Tsang's k_∞.

A similar disagreement with Tsang's high-pressure rates in cyclopentane[69] was reported by Kalra et al.[70] They studied dissociation of 0.2% and 1% cyclopentane in Ar mixed with 0.25% *tert*-butyl alcohol as internal comparators in the range 1185−1257 K. Cyclopentane dissociation was examined by Tsang[69] in the same temperature range, again with cyclohexene as an internal comparator. After comparing their observed ethylene, propene, and allene concentrations with the concentrations predicted in Tsang's experiments for similar conditions, Kalra et al.[70] concluded that Tsang's cyclohexene temperatures were consistently too high, amounting to about a 40 K discrepancy. They attributed this partially to the induced decomposition of the internal standard, cyclohexene, in Tsang's experiments and the remainder to the induced decomposition of cyclopentane in their own experiments. The comparator, isobutyl alcohol, used by Kalra et al.[70] can also dissociate through C−O and C−C bond fission

$$t\text{-}C_4H_9OH \rightarrow {}^{\bullet}t\text{-}C_4H_9 + {}^{\bullet}OH \quad (XVII)$$

$$t\text{-}C_4H_9OH \rightarrow {}^{\bullet}CH_3 + (CH_3)_2{}^{\bullet}COH \quad (XVIII)$$

along with the dominant isobutene formation channel

$$t\text{-}C_4H_9OH \rightarrow I\text{-}C_4H_8 + H_2O \quad (XIX)$$

Kalra et al.[70] argued that reactions XVII and XVIII would not alter the isobutene yield significantly, but the radicals formed in reactions XVII and XVIII could consume cyclopentane through abstraction reactions. On this basis, they estimated Tsang's reported temperatures to be 15−40 K higher than the actual values. As a correction to Tsang's rate constants, they suggested small upward adjustments of all pre-exponential factors keeping activation energies intact.[70] Introduction of a 15 K offset, the lower limit of the proposed error in Tsang's rate measurement, can increase the cyclopentane dissociation k_∞[69] by a factor of 1.6 at 1200 K. The above conclusion by Kalra et al.,[70] that Tsang has underestimated dissociation rate constants, was further supported by Brown et al.[15] in their own cyclopentane and cyclohexane dissociation study. Their estimated rate constants for cyclopentane and cyclohexane dissociation are 3−4 times higher than those of Tsang,[12,69] and those for cyclohexane are in good agreement with the k_∞ from the present study.

Some uncertainty in the rate constant of cyclohexene thermometer decomposition may well be the cause of this disagreement. Of course, use of a faster rate for the cyclohexene comparison reaction will increase the derived rate constant of cyclohexane dissociation (reaction 1). Skinner et al.,[71] used cyclohexene as an internal comparator for their own single-pulse shock tube study of ethane dissociation at 1000−1241 K and 3−9 atm, conditions comparable to those of Tsang.[12,69] The rate constant used for cyclohexene dissociation by Skinner et al.[71] is 1.5 times higher than that used by Tsang.[12,69] This problem may also occur with the internal comparator used for cyclohexane dissociation, 1-methylcyclohexene. Tsang reported absolute uncertainties of ±50% in the pre-exponential factor and of 0.96 kcal/mol in the activation energy of reaction XVII. Taking these uncertainties into account, the upper limit of the rate constant for reaction XVII can be 2.5 times higher than the rate constant used by Tsang.[12] The above observations serve to explain and perhaps justify the differences between Tsang's rate constants and our two RRKM extrapolated k_∞ values.

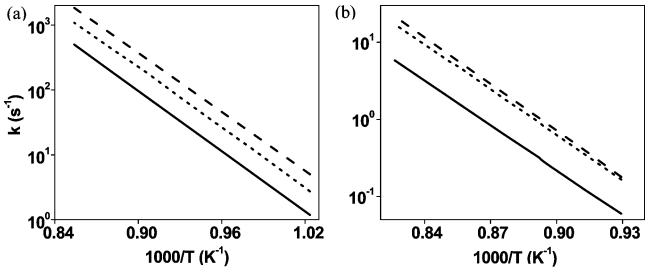

Figure 16. Comparison between the Tsang k_∞[12] and present RRKM model rate constants calculated for his experimental conditions in (a) 1-hexene and (b) cyclohexane: solid line, Tsang's k_∞; dashed line, k_∞ from the present work; dotted line, RRKM falloff rate constant calculated for Tsang's experimental pressures of 2−7 atm for cyclohexane and 2−6 atm for 1-hexene.

Conclusions

In this study we have measured rate constants for 1-hexene and cyclohexane dissociation at high temperatures and low pressures (for 1-hexene, $T = 1220-1700$ K, $P = 50$, 200 Torr; for cyclohexane, $T = 1400-2000$ K, $P = 25-200$ Torr) using the laser-schlieren technique. 1-Hexene mainly dissociates into allyl and *n*-propyl radicals through

$$1\text{-}C_6H_{12} \rightarrow CH_3CH_2CH_2^{\bullet} + {}^{\bullet}CH_2CH{=}CH_2 \qquad \Delta H_f^{298K} = 75.15 \text{ kcal/mol} \quad (2)$$

The LS technique cannot see the near thermoneutral retro-ene channel

$$1\text{-}C_6H_{12} \rightarrow CH_3CH{=}CH_2 + CH_3CH{=}CH_2 \qquad \Delta H_f^{298K} = 19.74 \text{ kcal/mol} \quad (X)$$

but little contribution from this or any other molecular channel is possible given the large positive and ultimately negative gradients generated by radical formation and recombination.

Cyclohexane itself predominantly isomerizes into 1-hexene:

$$c\text{-}C_6H_{12} \rightarrow 1\text{-}C_6H_{12} \quad (1)$$

Contributions from channels other than channel 1 were again neither needed nor indicated.

Using these two dominant dissociation channels, reactions 1 and 2, a reaction mechanism was developed which satisfactorily modeled the late time gradients associated with the secondary chemistry following the initial dissociation step in both precursors. The falloff rate constants obtained from the simulation of the experimental data were treated with RRKM theory, and k_∞ were estimated by extrapolation. The resulting k_∞ values are in close agreement with the experiments of Brown et al.[15] and the theoretical k_∞ obtained by Sirjean et al.[23] Disagreements with the k_∞ of Tsang[12] are probably a consequence of some uncompensated falloff and error in his thermometer rate. Of some interest is the large A factor in the cyclohexane rate expression, $k_\infty(1) = (8.76 \times 10^{17}) \exp((-91.94 \text{ kcal/mol})/RT)$ s^{-1}. However, if this is divided by the reaction-path degeneracy of 6, the result, 1.46×10^{17} s^{-1}, is very close to the same factor for central C−C scission in *n*-butane, 1.58×10^{17} s^{-1}, as given by Tsang.[72] This coincidence is certainly in accord with the notion of initial formation of a diradical by C−C fission in cyclohexane.

The "instantaneous" production of H-atoms reported by Braun-Unkhoff et al.[20] is actually readily explained by the H-forming reactions that occur immediately following 1-hexene dissociation

$$^{\bullet}C_3H_5 \rightarrow C_3H_4 + H \quad (6)$$

$$^{\bullet}C_3H_7 \rightarrow C_3H_6 + H \quad (5)$$

and the large quantities of C_2H_4 seen in the product analyses of Tsang[12] and Braun-Unkhoff et al.[20] are probably produced through the dominant route for the dissociation of *n*-propyl radicals

$$^{\bullet}C_3H_7 \rightarrow C_2H_4 + {}^{\bullet}CH_3 \quad (4)$$

No attempts were made to model the H-atom profiles or the C_2H_4 concentrations in either of these studies.

As noted above, 1-hexene formed in cyclohexane isomerization dissociates through reaction 2. The evidence for this two-step process, reaction 1 followed by reaction 2, is most clearly seen in Figure 7 and also weakly in Figure 8. However, at the lowest employed pressures and/or high temperatures, chemically activated 1-hexene molecules from cyclohexane may promptly dissociate and form allyl and *n*-propyl radicals without stabilization of the 1-hexene, i.e., following the one-step process, channel 1A. This process is hinted at by our low-pressure experiments (see Figures 12 and 13) but still cannot be clearly distinguished from the two-step process of reactions 1 and 2 because both ultimately produce the same products. In any case, the rates used for the one-step or the two-step model lie within the experimental uncertainty, and hence, the rate constant for cyclohexane dissociation at very low pressures is largely independent of the model assumed. On the basis of scatter, we would suggest that the present rates should apply with reasonable accuracy (±30%) throughout the current range of temperature and pressure.

Acknowledgment. The authors are indebted to N. K. Srinivasan for his help with the 1-hexene experiments. This work was supported by the U.S. Department of Energy, Office of Basic Energy Sciences, Division of Chemical Sciences, Geosciences and Biosciences, under Grant No. DE-FE-85ER13384 (J.H.K. and K.S.G.) and under Contract No. DE-AC02-06CH11357 (S.J.K. and L.B.H.).

Supporting Information Available: List of reactions and complete cyclohexane/1-hexene reaction mechanism. This material is available free of charge via the Internet at http://pubs.acs.org.

References and Notes

(1) Dawn, K. M.; Andrew, M.; Craig, A. T. *Phys. Today* **2008**, *61*, 47.
(2) Zhang, H. Z. R.; Huynh, L. K.; Kungwan, N.; Yang, Z. W.; Zhang, S. W. *J. Phys. Chem. A* **2007**, *111*, 4102.
(3) Cavallotti, C.; Rota, R.; Faravelli, T.; Ranzi, E. *Proc. Combust. Inst.* **2007**, *31*, 201.
(4) Law, M. E.; Westmoreland, P. R.; Cool, T. A.; Wang, J.; Hansen, N.; Taatjes, C. A.; Kasper, T. *Proc. Combust. Inst.* **2007**, *31*, 565.
(5) Silke, E. J.; Pitz, W. J.; Westbrook, C. K.; Ribaucour, M. *J. Phys. Chem. A* **2007**, *111*, 3761.
(6) Knepp, A. M.; Meloni, G.; Jusinski, L. E.; Taatjes, C. A.; Cavallotti, C.; Klippenstein, S. J. *Phys. Chem. Chem. Phys.* **2007**, *9*, 4315.
(7) Billaud, F.; Duret, M.; Elyahyaoui, K.; Baronnet, F. *Ind. Eng. Chem. Res.* **1991**, *30*, 1469.
(8) Yahyaoui, M.; Djebaili-Chaumeix, N.; Paillard, C. E.; Touchard, S.; Fournet, R.; Glaude, P. A.; Battin-Leclerc, F. *Proc. Combust. Inst.* **2005**, *30*, 1137.
(9) Yahyaoui, M.; Djebaïli-Chaumeix, N.; Dagaut, P.; Paillard, C. E.; Gail, S. *Combust. Flame* **2006**, *147*, 67.
(10) Miller, J. A.; Kee, P. J.; Westbrook, C. K. *Annu. Rev. Phys. Chem.* **1990**, *41*, 345.
(11) Gardiner, W. C. *Gas-Phase Combustion Chemistry*; Springer: New York, 2000.
(12) Tsang, W. *Int. J. Chem. Kinet.* **1978**, *10*, 1119.
(13) Aribike, D. S.; Susu, A. A.; Ogunye, A. F. *Thermochim. Acta* **1981**, *51*, 113.
(14) Aribike, D. S.; Susu, A. A.; Ogunye, A. F. *Thermochim. Acta* **1981**, *47*, 1.
(15) Brown, T. C.; King, K. D.; Nguyen, T. T. *J. Phys. Chem.* **1986**, *90*, 419.
(16) Voisin, D.; Marchal, A.; Reuillon, M.; Boettner, J. C.; Cathonnet, M. *Combust. Sci. Technol.* **1998**, *138*, 137.
(17) El-Bakali, A.; Braun-Unkhoff, M.; Dagaut, P.; Frank, P.; Cathonnet, M. *Proc. Combust. Inst.* **2000**, *28*, 1631.
(18) Granata, S.; Faravelli, T.; Ranzi, E. *Combust. Flame* **2003**, *132*, 533.
(19) McEnally, C. S.; Pfefferle, L. D. *Combust. Flame* **2004**, *136*, 155.
(20) Braun-Unkhoff, M.; Naumann, C.; Frank, P. *Abstr. Pap.—Am. Chem. Soc.* **2004**, *227*, U1096.
(21) Sirjean, B.; Buda, F.; Hakka, H.; Glaude, P. A.; Fournet, R.; Warth, V.; Battin-Leclerc, F.; Ruiz-Lopez, M. *Proc. Combust. Inst.* **2007**, *31*, 277.
(22) Lemaire, O.; Ribaucour, M.; Carlier, M.; Minetti, R. *Combust. Flame* **2001**, *127*, 1971.

(23) Sirjean, B.; Glaude, P. A.; Ruiz-Lopez, M. F.; Fournet, R. *J. Phys. Chem. A* **2006**, *110*, 12693.
(24) King, K. D. *Int. J. Chem. Kinet.* **1979**, *11*, 1071.
(25) Glaude, P. A.; Warth, V.; Fournet, R.; Battin-Leclerc, F.; Scacchi, G.; Come, G. M. *Int. J. Chem. Kinet.* **1998**, *30*, 949.
(26) Fournet, R.; Battin-Leclerc, F.; Glaude, P. A.; Judenherc, B.; Warth, V.; Come, G. M.; Scacchi, G.; Ristori, A.; Pengloan, G.; Dagaut, P.; Cathonnet, M. *Int. J. Chem. Kinet.* **2001**, *33*, 574.
(27) Kiefer, J. H.; Manson, A. C. *Rev. Sci. Instrum.* **1981**, *52*, 1392.
(28) Kiefer, J. H. The Laser-Schlieren Technique in Shock Tube Kinetics. In *Shock Waves in Chemistry*; Lifshitz, A., Ed.; Marcel Dekker: New York, 1981; p 219.
(29) Santhanam, S.; Kiefer, J. H.; Tranter, R. S.; Srinivasan, N. K. *Int. J. Chem. Kinet.* **2003**, *35*, 381.
(30) Srinivasan, N. K.; Kiefer, J. H.; Tranter, R. S. *J. Phys. Chem. A* **2003**, *107*, 1532.
(31) Kiefer, J. H.; Kumaran, S. S.; Sundaram, S. *J. Chem. Phys.* **1993**, *99*, 3531.
(32) Burcat, A.; Ruscic, B. Ideal Gas Thermochemical Database with Updates from Active Thermochemical Tables, 2008. ftp://ftp.technion.ac.il/pub/supported/aetdd/thermodynamics.
(33) *CRC Handbook of Chemistry and Physics*, 57th ed.; CRC Press: Cleveland, OH, 1976−1977.
(34) Gardiner, W. C.; Hidaka, Y.; Tanzawa, T. *Combust. Flame* **1981**, *40*, 213.
(35) Tsang, W. *J. Phys. Chem. A* **2006**, *110*, 8501.
(36) Tsang, W.; Bedanov, V.; Zachariah, M. R. *J. Phys. Chem.* **1996**, *100*, 4011.
(37) Just, T. *Proc. Combust. Inst.* **1994**, *25*, 687.
(38) Tsang, W. *Ind. Eng. Chem. Res.* **1992**, *31*, 3.
(39) Tsang, W.; Hampson, R. F. *J. Phys. Chem. Ref. Data* **1986**, *15*, 1087.
(40) Baulch, D. L.; Cobos, C. J.; Cox, R. A.; Esser, C.; Frank, P.; Just, T.; Kerr, J. A.; Pilling, M. J.; Troe, J.; Walker, R. W.; Warnatz, J. *J. Phys. Chem. Ref. Data* **1992**, *21*, 411.
(41) Wang, H.; You, X.; Joshi, A. V.; Davis, S. G.; Laskin, A.; Egolfopoulos, F.; Law, C. K. USC Mech Version II. High-Temperature Combustion Reaction Model of H2/CO/C1-C4 Compounds, May 2007. http://ignis.usc.edu/USC_Mech_II.htm.
(42) Baboul, A. G.; Curtiss, L. A.; Redfern, P. C.; Raghavachari, K. *J. Chem. Phys.* **1999**, *110*, 7650.
(43) Frisch, M. J.; Trucks, G. W.; Schlegel, H. B.; Scuseria, G. E.; Robb, M. A.; Cheeseman, J. R.; Montgomery, J. A., Jr.; Vreven, T.; Kudin, K. N.; Burant, J. C.; Millam, J. M.; Iyengar, S. S.; Tomasi, J.; Barone, V.; Mennucci, B.; Cossi, M.; Scalmani, G.; Rega, N.; Petersson, G. A.; Nakatsuji, H.; Hada, M.; Ehara, M.; Toyota, K.; Fukuda, R.; Hasegawa, J.; Ishida, M.; Nakajima, T.; Honda, Y.; Kitao, O.; Nakai, H.; Klene, M.; Li, X.; Knox, J. E.; Hratchian, H. P.; Cross, J. B.; Bakken, V.; Adamo, C.; Jaramillo, J.; Gomperts, R.; Stratmann, R. E.; Yazyev, O.; Austin, A. J.; Cammi, R.; Pomelli, C.; Ochterski, J. W.; Ayala, P. Y.; Morokuma, K.; Voth, G. A.; Salvador, P.; Dannenberg, J. J.; Zakrzewski, V. G.; Dapprich, S.; Daniels, A. D.; Strain, M. C.; Farkas, O.; Malick, D. K.; Rabuck, A. D.; Raghavachari, K.; Foresman, J. B.; Ortiz, J. V.; Cui, Q.; Baboul, A. G.; Clifford, S.; Cioslowski, J.; Stefanov, B. B.; Liu, G.; Liashenko, A.; Piskorz, P.; Komaromi, I.; Martin, R. L.; Fox, D. J.; Keith, T.; Al-Laham, M. A.; Peng, C. Y.; Nanayakkara, A.; Challacombe, M.; Gill, P. M. W.; Johnson, B.; Chen, W.; Wong, M. W.; Gonzalez, C.; Pople, J. A. *Gaussian 03*, revision C.02; Gaussian, Inc.: Wallingford, CT, 2004.
(44) Miller, J. A.; Klippenstein, S. J. *Phys. Chem. Chem. Phys.* **2004**, *6*, 1192.
(45) Bencsura, A.; Knyazev, V. D.; Xing, S. B.; Slagle, I. R.; Gutman, D. *Proc. Combust. Inst.* **1992**, *24*, 629.
(46) Curran, H. J. *Int. J. Chem. Kinet.* **2006**, *38*, 250.
(47) Kiefer, J. H.; Santhanam, S.; Srinivasan, N. K.; Tranter, R. S.; Klippenstein, S. J.; Oehlschlaeger, M. A. *Proc. Combust. Inst.* **2005**, *30*, 1129.
(48) Gupte, K. S.; Kiefer, J. H.; Tranter, R. S.; Klippenstein, S. J.; Harding, L. B. *Proc. Combust. Inst.* **2007**, *31*, 167.
(49) Saxena, S.; Kiefer, J. H.; Klippenstein, S. J. *Proc. Combust. Inst.* **2009**, *32*, 123.
(50) Yang, X.; Goldsmith, C. F.; Tranter, R. S. Submitted for publication to *J. Phys. Chem. A*.
(51) Yang, X.; Jasper, A. W.; Kiefer, J. H.; Tranter, R. S. Submitted for publication to *J. Phys. Chem. A*.
(52) Fernandes, R. X.; Giri, B. R.; Hippler, H.; Kachiani, C.; Striebel, F. *J. Phys. Chem. A* **2005**, *109*, 1063.
(53) NIST Computational Chemistry Comparison and Benchmark Database, NIST Standard Reference Database Number 101, release 14; Johnson, R. D., III., Ed.; Sept 2006. http://srdata.nist.gov/cccbdb.
(54) Dean, A. M. *J. Phys. Chem.* **1985**, *89*, 4600.
(55) Andersson, M. P.; Uvdal, P. *J. Phys. Chem. A* **2005**, *109*, 2937.
(56) Kiefer, J. H.; Buzyna, L. L.; Dib, A.; Sundaram, S. *J. Chem. Phys.* **2000**, *113*, 48.
(57) Cottrell, T. L.; McCoubrey, J. C. *Molecular Energy Transfer in Gases*; Butterworths: London, 1961.
(58) Kiefer, J. H.; Alalami, M. Z.; Hajduk, J. C. *Appl. Opt.* **1981**, *20*, 221.
(59) Kiefer, J. H.; Shah, J. N. *J. Phys. Chem.* **1987**, *91*, 3024.
(60) Harding, L. B.; Georgievskii, Y.; Klippenstein, S. J. *J. Phys. Chem. A* **2005**, *109*, 4646.
(61) Tsang, W. *J. Phys. Chem. Ref. Data* **1988**, *17*, 887.
(62) Scherzer, K.; Loeser, U.; Stiller, W. *Z. Chem.* **1987**, *27*, 300.
(63) Tsang, W. *J. Phys. Chem. Ref. Data* **1991**, *20*, 221.
(64) Iwan, I.; McGivern, W. S.; Manion, J. A.; Tsang, W. *Proceedings of the 5th U.S. Combustion Meeting*, San Diego, CA, 2007; CO2.
(65) Forst, W. *Unimolecular Reactions: A Concise Introduction*; Cambridge University Press: Cambridge, U.K., New York, 2003.
(66) Oref, I.; Tardy, D. C. *Chem. Rev.* **1990**, *90*, 1407.
(67) Tranter, R. S.; Brezinsky, K.; Fulle, D. *Rev. Sci. Instrum.* **2001**, *72*, 3046.
(68) Throssell, J. J. *Int. J. Chem. Kinet.* **1972**, *4*, 273.
(69) Tsang, W. *Int. J. Chem. Kinet.* **1978**, *10*, 599.
(70) Kalra, B. L.; Feinstein, S. A.; Lewis, D. K. *Can. J. Chem.* **1979**, *57*, 1324.
(71) Skinner, G. B.; Rogers, D.; Patel, K. B. *Int. J. Chem. Kinet.* **1981**, *13*, 481.
(72) Tsang, W. *Int. J. Chem. Kinet.* **1978**, *10*, 821.

JP905891Q